BASIC RESEARCH PAPER

Autophagy 10:8, 1426–1441; August 2014; © 2014 Landes Bioscience

Coronavirus NSP6 restricts autophagosome expansion

Eleanor M Cottam, Matthew C Whelband, and Thomas Wileman*

Norwich Medical School; University of East Anglia; Norwich UK

Keywords: autophagosome quantification, autophagy, coronavirus, MHV, nonstructural proteins, omegasome, SARS

Abbreviations: ATG, autophagy-related; BECN1, Beclin 1, autophagy related; DMV, double-membraned vesicle; ER, endoplasmic reticulum; GFP, green fluorescent protein; HBSS, Hank's balanced salt solution; IBV, infectious bronchitis virus; LAMP2, lysosomal-associated membrane protein 2; LC3-II, LC3-phosphatidylethanolamine conjugate; MAP1LC3B, microtubule-associated protein 1 light chain 3 beta; MHV, mouse hepatitis virus; MTOR, mechanistic target of rapamycin; MTORC1, mechanistic target of rapamycin complex 1; NSP, nonstructural protein; PIK3C3, phosphatidylinositol 3-kinase, catalytic subunit type 3; PRRSV, porcine reproductive and respiratory syndrome virus; PtdIns, phosphatidylinositol; RB1CC1, RB1-inducible coiled-coil 1; SARS, severe acute repiratory syndrome; SQSTM1, sequestosome 1; UKC, ULK1, ATG13, RB1CC1, and ATG101 complex; ULK1, unc-51 like autophagy activating kinase 1; WIPI2, WD repeat domain, phosphoinositide interacting 2; ZFYVE1, zinc finger, FYVE domain containing 1

Autophagy is a cellular response to starvation that generates autophagosomes to carry long-lived proteins and cellular organelles to lysosomes for degradation. Activation of autophagy by viruses can provide an innate defense against infection, and for (+) strand RNA viruses autophagosomes can facilitate assembly of replicase proteins. We demonstrated that nonstructural protein (NSP) 6 of the avian coronavirus, infectious bronchitis virus (IBV), generates autophagosomes from the ER. A statistical analysis of MAP1LC3B puncta showed that NSP6 induced greater numbers of autophagosomes per cell compared with starvation, but the autophagosomes induced by NSP6 had smaller diameters compared with starvation controls. Small diameter autophagosomes were also induced by infection of cells with IBV, and by NSP6 proteins of MHV and SARS and NSP5, NSP6, and NSP7 of arterivirus PRRSV. Analysis of WIPI2 puncta induced by NSP6 suggests that NSP6 limits autophagosome diameter at the point of omegasome formation. IBV NSP6 also limited autophagosome and omegasome expansion in response to starvation and Torin1 and could therefore limit the size of autophagosomes induced following inhibition of MTOR signaling, as well as those induced independently by the NSP6 protein itself. MAP1LC3B-puncta induced by NSP6 contained SQSTM1, which suggests they can incorporate autophagy cargos. However, NSP6 inhibited the autophagosome/lysosome expansion normally seen following starvation. Taken together the results show that coronavirus NSP6 proteins limit autophagosome expansion, whether they are induced directly by the NSP6 protein, or indirectly by starvation or chemical inhibition of MTOR signaling. This may favor coronavirus infection by compromising the ability of autophagosomes to deliver viral components to lysosomes for degradation.

Introduction

Autophagy provides a short-term supply of amino acids in response to starvation by delivering damaged organelles and long-lived proteins to lysosomes for degradation. Autophagy begins with the nucleation of phagophores, which then expand to form double-membrane autophagosomes able to sequester portions of the cytosol.[1] Autophagy is initiated by sequential interactions between the nutrient-sensing MTOR kinase and ULK1 protein complex (UKC). UKC is a complex of ULK1, ATG13, RB1CC1/FIP200, and ATG101. In nutrient-rich conditions MTOR is active and phosphorylates ATG13 within the UKC. However, following starvation or nutrient depletion MTOR is inactivated, and ULK1 increases phosphorylation of RB1CC1. These changes enable the UKC to bind a second protein complex containing BECN1/Vps30/Atg6, ATG14, and a class 3 phosphatidylinositol 3-kinase, whose catalytic subunit is termed PIK3C3.[2]

The endoplasmic reticulum (ER) is one of several sources of lipids for autophagosome formation. Anchoring of ATG14 to the ER[3] and/or ER-mitochondrial contact sites,[4] plays a key role in recruiting the BECN1-ATG14-PIK3C3 complex from the cytosol to sites of autophagosome formation in response to starvation. Localized phosphorylation of lipids by PIK3C3 generates ER domains called omegasomes enriched in phosphatidylinositol-3-phosphate (PtdIns3P) that recruit PtdIns3P-effector proteins such as WIPI1/2 to generate sites able to prime phagophore

*Correspondence to: Thomas Wileman; Email: T.Wileman@uea.ac.uk
Submitted: 04/26/2013; Revised: 05/12/2014; Accepted: 05/21/2014; Published Online: 06/11/2014
http://dx.doi.org/10.4161/auto.29309

formation and expansion.[5-7] The omegasome was first identified by analyzing the translocation of ZFYVE1/DFCP1 to punctate structures aligned along the ER.[5] ZFYVE1 binds to PtdIns3P and can be used to identify the omegasome and subsequent autophagosome. The activated PIK3C3-BECN1 complex also promotes ubiquitin-like reactions, which generate an ATG12–ATG5-ATG16 conjugate, and add phosphatidylethanolamine (PE) to MAP1LC3B/ATG8. Recruitment of the MAP1LC3B–PE conjugate (also known as LC3-II) results in phagophore expansion and eventual release of autophagosomes into the cytosol. LC3-II is the major protein of the autophagosome and remains with the autophagosome until fusion with the lysosomes.[8,9] For this reason immunodetection, or green fluorescent protein (GFP) tagging of MAP1LC3 has become indispensable for visualizing autophagosomes in mammalian cells.

The capacity to degrade large quantities of cytoplasm provides cells with a powerful means of killing intracellular pathogens and increasing presentation of microbial components to the immune system.[10] Autophagy provides an innate immune defense against viruses by delivering viruses and viral proteins to lysosomes for degradation. For example, Herpes simplex 1, vesicular stomatitis, and Sindbis viruses are susceptible to autophagy, and inhibition of autophagy leads to increased replication and virulence.[11-13] In contrast, autophagy can promote infection by picornaviruses, such as poliovirus and coxsackieviruses, because autophagosomes provide sites for replication.[14-17] The observation that autophagy can affect viral infection in different ways has stimulated a search for viral proteins that can modulate autophagy. The ICP34.5 protein of Herpes simplex 1 virus, for example, inhibits autophagy by binding BECN1 and is linked to neurovirulence 'in vivo'.[18] For picornaviruses the 2BC protein of poliovirus induces recruitment of MAP1LC3 to membranes, and in the presence of poliovirus 3A protein, generates autophagosomes.[19,20] Hepatitis C NS4B induces autophagosomes through a pathway requiring RAB5A and PIK3C3,[21] while vesicular stomatitis virus G protein,[22] the p17 of avian reovirus[23] and SV40 small T antigen[24] activate autophagy by inhibition of the MTOR kinase through downregulation of AKT signaling.

Infectious bronchitis virus (IBV) is an avian coronavirus that causes major losses to the poultry industry. In common with mammalian coronaviruses such as mouse hepatitis virus (MHV) and severe respiratory syndrome coronavirus (SARS), IBV is a large positive sense RNA virus where two-thirds of the genome encodes nonstructural proteins (NSP) needed for virus replication.[25] Many of the NSPs are assembled into a replication complex on the cytoplasmic face of the ER. Replicase assembly and genome replication are coincident with the formation of large numbers of closely packed double-membrane vesicles at sites of replication, and activation of autophagy.[26,27] We have searched for coronavirus proteins that activate autophagy and have shown that autophagy can be induced by NSP6 of IBV, MHV, and SARS, and also by the equivalent NSP5-7 ortholog encoded by porcine reproductive and respiratory syndrome virus (PRRSV).[28] These proteins have multiple membrane-spanning domains and locate to the ER where they activate autophagy through a pathway dependent on ATG5 and PIK3C3. Many features of autophagy induction by NSP6 suggested that the protein activates the omegasome pathway normally used by cells to generate autophagosomes from the ER in response to starvation. Expression of NSP6 proteins results in increased levels of Ptdlns3P on ER membranes, recruitment of Ptdlns3P effector protein WIPI2 and the generation of autophagosomes directly from the ER. In this paper we have investigated the properties of autophagosomes generated by coronavirus NSP6 proteins, and IBV infection, and compared them with autophagosomes induced by starvation. We found that the coronavirus NSP6 protein limits the expansion of autophagosomes either produced directly by NSP6, or indirectly following starvation or chemical inhibition of MTOR signaling. Inhibition occurs at the stage of omegasome formation and as a result prevents the formation of large autolysosomes.

Results

Coronavirus NSP6 proteins, and IBV, generate small diameter autophagosomes

Coronavirus NSP6 proteins are multiple-spanning transmembrane proteins that locate to the ER where they induce autophagosomes via an omegosome intermediate.[28] **Figure 1** shows a side-by-side comparison of autophagosomes formed in response to starvation (**Fig. 1A**) with autophagosomes formed by NSP6 from IBV (**Fig. 1B**), or MHV (**Fig. 1C**) fused to mCherry. NSP6 proteins were identified through reticular ER distribution of mCherry signal (pseudocolored black in **Fig. 1B and C**). Cells were immmunolabeled for endogenous MAP1LC3B and pixel densities of MAP1LC3B puncta present in the z stacks were rendered into spherical spots by Imaris software allowing statistical analysis (see Materials and Methods for details). The diameters of puncta were color coded using a heat map where blue represents puncta less than 0.3 μm in diameter, green those of about 0.5 μm, and red puncta 1 μm or more in diameter. MAP1LC3B puncta formed in response to starvation were mainly red indicating diameters of ≥ 1 μm. The size of mature autophagosomes calculated from electron micrographs is around 1 μm, so the pixel rendering analysis generating red spheres correlates well with accepted dimension of autophagosomes.[29] The puncta generated by IBV and MHV NSP6 were predominantly green or blue (≤ 0.5 μm diameter) suggesting that MAP1LC3B puncta induced by NSP6 proteins were of small diameter and/or that NSP6 slowed autophagosome expansion. MAP1LC3B puncta generated by the NSP6, or equivalent protein, SARS virus, and PRRSV were also analyzed (**Fig. S1**). Images were compared by observing cells expressing equivalent fluorescent signals from the RFP-tagged NSP6 and ensuring that NSP6 generated a reticular stain indicative of translocation to the endoplasmic reticulum. In each case MAP1LC3B puncta were ≤ 0.5 μm diameter.

The experiment was repeated for cells infected with IBV (**Fig. 1D**). In the absence of an antibody against NSP6, infected cells were detected by immunostaining for double-stranded RNA (pseudocolored black in **Fig. 1D**). Cells negative for dsRNA had very few MAP1LC3B puncta. Large numbers of puncta were formed in infected cells, and as seen for NSP6, the majority were

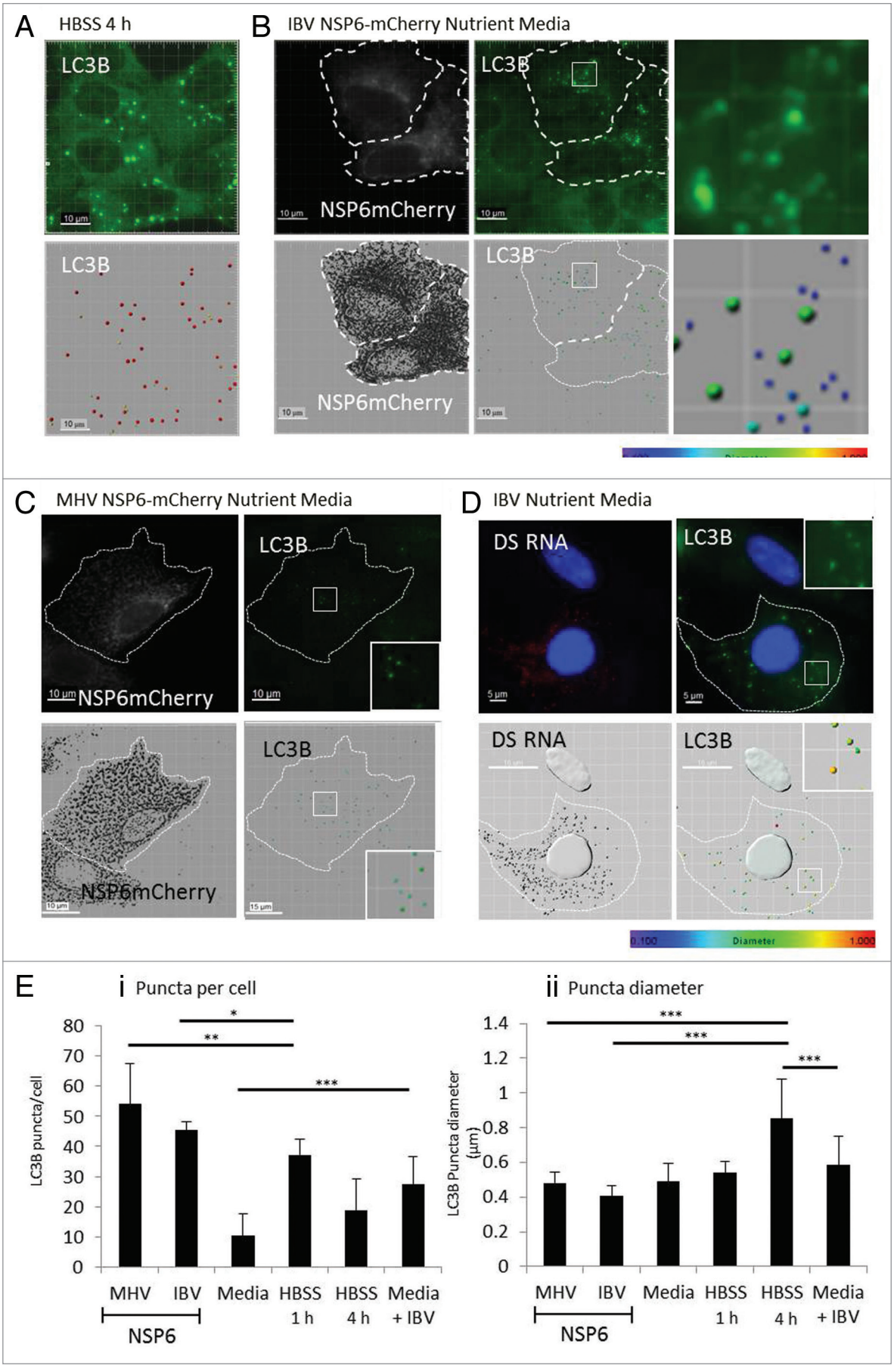
A
HBSS 4 h
LC3B
LC3B
B
IBV NSP6-mCherry Nutrient Media
LC3B
NSP6mCherry
LC3B
LC3B
NSP6mCherry
LC3B
C
MHV NSP6-mCherry Nutrient Media
NSP6mCherry
LC3B
NSP6mCherry
LC3B
D
IBV Nutrient Media
DS RNA
LC3B
DS RNA
LC3B
Diameter
E
i Puncta per cell
LC3B puncta/cell
MHV
IBV
Media
HBSS 1 h
HBSS 4 h
Media + IBV
NSP6
ii Puncta diameter
LC3B Puncta diameter (μm)
MHV
IBV
Media
HBSS 1 h
HBSS 4 h
Media + IBV
NSP6

Figure 1 (See opposite page). Analysis of autophagosomes induced by coronavirus NSP6 proteins or infection with infectious bronchitis virus. Autophagosomes were visualized in Vero cells by immunofluorescence staining for endogenous MAP1LC3B. Pixel densities in fluorescent images were analyzed in Imaris using spot function to generate rendered images. The diameters of MAP1LC3B-puncta were color coded using a heat map where blue represents puncta less than 3.0 μm, green puncta are 0.5 μm and red puncta 1.0 μm or greater. (**A**) cells starved in HBSS for 4 h. (**B**) cells expressing IBV NSP6-mCherry. (**C**) cells expressing MHV NSP6-mCherry. (**D**) cells imaged after overnight infection with IBV. Infected cells were detected by immunostaining for double-stranded RNA (dsRNA). Rendered images are shown below the fluorescence micrographs, the images are projections made of 9 z slices 300 nm apart. Cells expressing NSP6-mCherry, or infected with IBV are outlined with white hatched lines, mCherry signals and dsRNA are pseudocolored in black in rendered images. (**E**) Composite data calculated from from 3 replicate experiments. MHV NSP6: 867 puncta from 16 cells, IBV NSP6: 1137 puncta from 26 cells, IBV infection: 590 puncta from 24 cells, nutrient media control: 380 puncta from 21 cells, HBSS 1 h: 845 puncta from 23 cells, HBSS 4 h: 421 puncta from 25 cells. Significant differences in puncta per cell and puncta diameter were measured by a paired *t* test. ***A significant difference of $P < 0.0001$ ** A significant difference of $P < 0.001$* A significant difference of $P < 0.01$.

rendered into green spheres suggesting small diameter. Data from 3 replicate experiments analyzing a minimum of 25 cells are presented in **Figure 1E**. Expression of MHV or IBV NSP6 protein resulted in a small but significant ($P < 0.01$) increase in number of puncta per cell (= 54, σ = 15.07, and = 45, σ = 13.3) respectively, when compared with 1 h starvation in HBSS (= 37, σ = 7.2), but the puncta generated by MHV NSP6 or IBV NSP6 had smaller diameter (= 0.45 μm, σ = 0.11) when compared with starvation (= 0.85 μm, σ = 0.22). Autophagosomes induced by IBV infection were also smaller (= 0.58 μm, σ = 0.17) than those induced through starvation (= 0.85 μm, σ = 0.22), although not as small as those observed with IBV NSP6 (= 0.45 μm, σ = 0.11).

Extent of autophagosome expansion is dependent on the time course of starvation

In the above experiments small diameter autophagosomes were generated in cells expressing NSP6 proteins maintained in nutrient-rich media. This made it possible that NSP6 proteins have an inherent ability to limit autophagosome expansion, or that autophagosomes are unable to expand in cells maintained in nutrient media. The latter was tested by first analyzing the numbers and diameters of autophagosomes in control cells at increasing times after transfer to HBSS (**Fig. 2A**). The numbers of MAP1LC3B-positive puncta increased over the first 60 min and the majority were rendered in green indicating diameters ~0.5 μm. At later times (120 to 180 min) numbers of MAP1LC3B puncta decreased, but their average diameter increased above 0.5 μm as indicated by appearance of yellow, orange, and red spheres in rendered images. Numbers and sizes of MAP1LC3B puncta from 3 replicate experiments are shown in **Figure 2B**. To estimate the numbers of larger autophagosomes, it was decided to use a numerical cut off of 0.75 μm, as not all autophagosomes after 4 h starvation were greater than 1 μm in diameter; however, 0.75 μm was outside the standard deviation range of autophagosome diameters seen under nutrient-media conditions. In nutrient media (0 min) there were a mean of 18 puncta per cell and these were small (= 0.49 μm, σ = 0.11 in diameter) with just 2.4% ≥ 0.75 μm. Following starvation numbers of puncta peaked at 60 min with a mean of 37 per cell, and then dropped to a mean of 18.6 after 4 h. The percentage of larger puncta with diameters of ≥ 0.75 μm remained low (9.8%) for the first h of starvation but increased to 73.2%, between 2 and 3 h and decreased to 56.4% at 5 h.

Mature autophagosomes are reported to be approximately 1 μm in diameter.[29] The results suggest that autophagosomes formed during the first h of starvation were unable to mature, or that it takes between 1 and 2 h for autophagosomes to reach diameters ≥ 0.75 μm. This was tested directly by comparing time-lapse images of GFP-MAP1LC3B puncta taken at early or late times following starvation. Adenovirus transduction was used to express GFP-MAP1LC3B and the diameters of GFP puncta were comparable to endogenous immunostained MAP1LC3B puncta as measured by Imaris (data not shown). GFP-MAP1LC3B puncta formed in nutrient media (**Fig. 2C**) showed blue-green transition within 3 min suggesting a diameter of 0.5 μm, and remained this size before disappearing (**Vid. S1**). GFP-MAP1LC3B puncta formed between 1 and 2 h (**Fig. 2D**; **Vid. S2**) grew rapidly and could reach diameters greater than 0.75 μm (orange) within 5 min. After 2 h in HBSS, vesicles were able to grow until over 1 μm in diameter (red) within 5 min of forming (**Fig. 2E**; **Vid. S3**). **Figure 2F** shows analysis of GFP-MAP1LC3B puncta generated from the ER by IBV NSP6. The GFP-puncta induced by NSP6 showed blue to green transition but did not grow larger than 0.5 μm diameter and then faded within 6 min (**Vid. S4**).

IBV infection and IBV NSP6 expression limit expansion of autophagosomes generated in response to starvation or inhibition of MTOR kinase

The experiments above showed that when autophagosomes were formed in nutrient media, or during the first h following transfer to HBSS, they were unable to expand to diameters ≥ 1 μm. This made it possible that incubation in nutrient media, rather than properties inherent to NSP6, limited the diameter of GFP puncta in cells expressing NSP6. The next experiment therefore analyzed the effect of IBV NSP6-mCherry on the diameters of autophagosomes induced in cells maintained in HBSS to induce starvation. **Figure 3A**, **i** compares endogenous MAP1LC3B puncta in cells expressing NSP6 (indicated by white outline in **Fig. 3A**, **i**) with those in cells negative for NSP6, 4 h following transfer to HBSS. The rendered images in the lower panels show that endogenous MAP1LC3B puncta within cells expressing NSP6-mCherry were smaller (green and blue) than those in cells negative for NSP6 (red and orange). **Figure 3A**, **ii** shows a similar analysis of cells infected with IBV while **Figure 3A**, **iii** shows cells incubated with Torin1 to inhibit MTOR kinase. The charts in **Figure 3B** show analysis of a minimum of 25 cells per condition and count puncta per cell, and mean puncta diameter. The diameters of endogenous MAP1LC3B puncta in response to starvation in cells expressing NSP6, or infected with IBV, remained less than 1 μm (0.48 μm), and significantly smaller on average than control starved cells (≥ 0.75 μm). NSP6 was therefore able to limit the expansion of autophagosomes induced

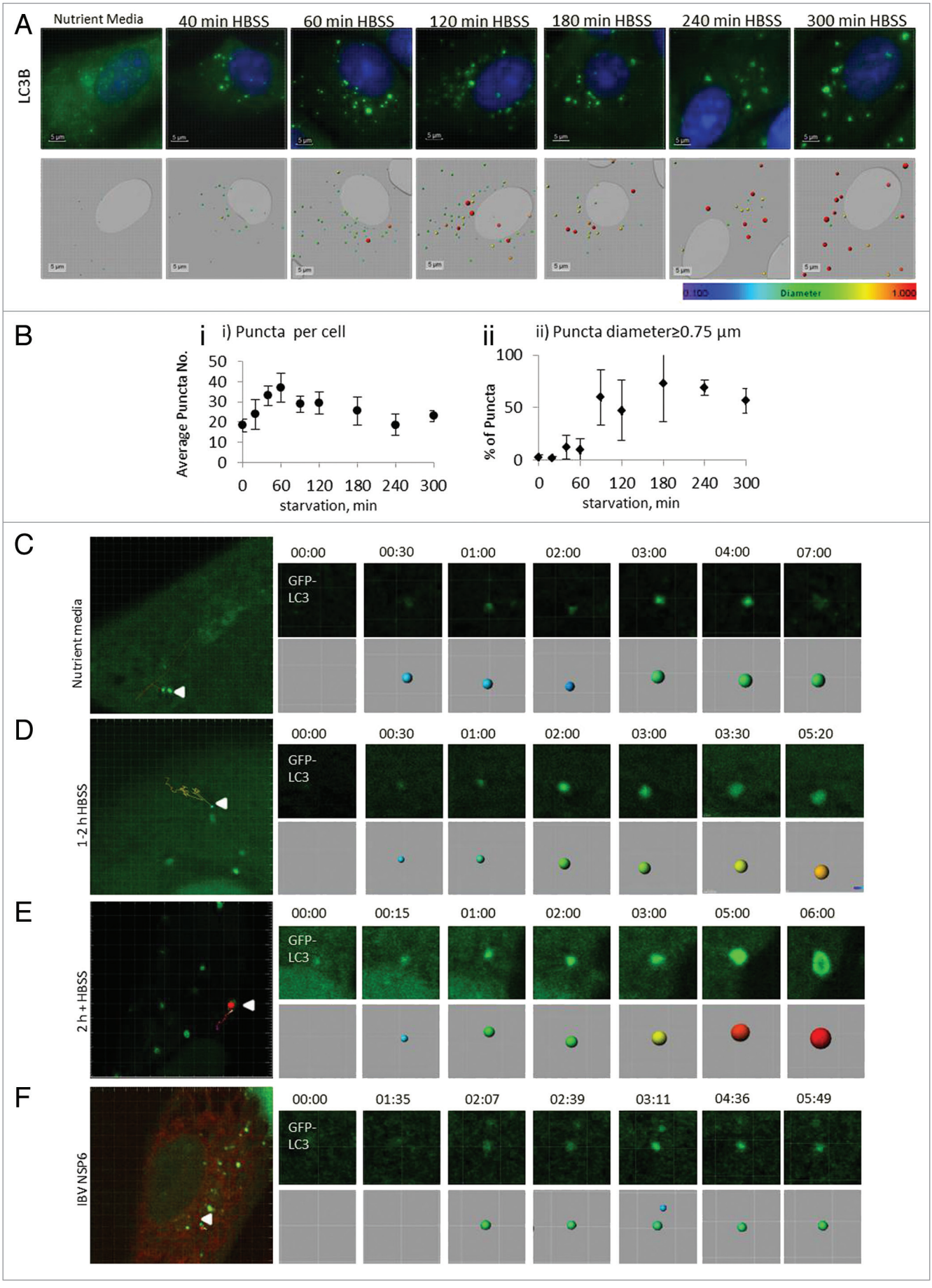
A
Nutrient Media
40 min HBSS
60 min HBSS
120 min HBSS
180 min HBSS
240 min HBSS
300 min HBSS
LC3B
Diameter
B
i) Puncta per cell
Average Puncta No.
starvation, min
ii) Puncta diameter≥0.75 µm
% of Puncta
starvation, min
C
Nutrient media
GFP-LC3
D
1-2 h HBSS
GFP-LC3
E
2 h + HBSS
GFP-LC3
F
IBV NSP6
GFP-LC3

Figure 2 (See opposite page). Effect of HBSS on autophagosome maturation. (**A**) Analysis of autophagosome expansion during starvation. Vero cells were transferred from nutrient media to HBSS and fixed at the indicated times. Autophagosomes were visualized by immunofluorescence staining for endogenous MAP1LC3B. Pixel densities in fluorescent images were analyzed in Imaris using spot function to generate rendered images presented below the corresponding fluorescent images (the images are projections made of 9 z slices 300 nm apart). The diameters of MAP1LC3B-puncta were color coded using a heat map where blue represents puncta less than 3.0 μm, green puncta are 0.5 μm and red puncta 1.0 μm or greater. The images show examples from 3 replicate experiments. (**B**) Analysis of autophagosome numbers and diameters during starvation. The number of puncta per cell was calculated from ≥ 20 cells per time point taken from 3 starvation time courses and plotted with the error bars representing the standard deviation (left chart). The percentage of puncta identified with a diameter ≥ 0.75 μm was also calculated and plotted over time (right chart). (**C–G**) Time-lapse imaging of autophagosome lifetime. Vero cells were transduced with an adenovirus expressing mammalian GFP-MAP1LC3B. The following day the cells were transferred to HBSS and the time course of GFP-MAP1LC3B puncta formation and decay was determined by time-lapse imaging. GFP-MAP1LC3B puncta were tracked and analyzed using Imaris spot and surface functions. The left-hand image on each panel identifies the autophagosome of interest and shows its track as determined by Imaris. Color-coded rendered images are shown below corresponding fluorescence images from example time points indicated in min. (**C**) nutrient media. (**D**) 1 to 2 h after transfer to HBSS. (**E**) 4 h after transfer to HBSS. (**F**) cells in nutrient media expressing IBV NSP6 mCherry.

by starvation or inhibition of MTOR by Torin1, and diameters remained close to 0.5 μm.

The effect of NSP6 on autophagosome expansion was examined further by compiling data from live-cell imaging of GFP-MAP1LC3B-puncta. Each of the data points in **Figure 3C** represent individual GFP-MAP1LC3B puncta in terms of life time (*y* axis seconds) and maximum diameter (*x* axis); the vertical line indicates a diameter of 0.75 μm. Consistent with the results above, GFP-MAP1LC3B puncta in nutrient media, and cells starved for 1 h were short-lived with maximum diameters less than 0.75 μm (**Fig. 3C**, **i and ii**). GFP-MAP1LC3B puncta with diameters greater than 0.75 μm (indicated to the right of the vertical line) formed between 1 and 3 h of starvation and 10% of these showed increased lifetimes (**Fig. 3C**, **iii**). Those generated after 3 h were mostly greater 0.75 μm diameter, but these did not show increases in lifetime (**Fig. 3C**, **iv**). In cells expressing NSP6 GFP-MAP1LC3B puncta failed to increase in size following starvation, or show increased lifetime (**Fig. 3C**, **v–viii**). Taken together these 2 approaches showed that NSP6 has an ability to limit the diameter of autophagosomes induced by starvation or by chemical inhibition of MTOR kinase.

IBV NSP6 protein limits expansion of omegasomes

Omegasomes are sites on ER cisternae where localized production of PtdIns3P provides a platform for the recruitment of proteins that will eventually form autophagsomes. WIPI2 binds PtdIns3P and colocalizes with ZFYVE1-GFP during autophagosome formation and is a marker for omegasomes.[7] This allowed us to use an analysis of WIPI2 puncta to follow the effects of NSP6 on omegasome expansion. **Figure 4A** shows examples of immunostained endogenous WIPI2 puncta and corresponding rendered images for cells expressing IBV NSP6-mCherry in nutrient media (**Fig. 4A**, **i**) and cells expressing IBV NSP6-mCherry and starved for 4 h (**Fig. 4A**, **ii**), and control cells starved in HBSS (**Fig. 4A**, **iii**). Numbers and sizes of WIPI2 puncta were assessed from 3 replicate experiments to produce the charts in **Figure 4B**. During a starvation time course (**Fig. 2B**, **i and ii**), numbers of WIPI2 puncta per cell increased between 1 and 2 h (= 6.7, σ = 0.98 to = 19.6, σ = 9.7) per cell, and then decreased (= 14.7, σ = 3.1) after 3 h. As seen for endogenous MAP1LC3B (**Fig. 2A and B**), significant numbers of WIPI2 puncta ≥ 0.75 μm diameter were first seen at 2 h (20%), increased to 58% at 3 h, and then decreased to 20% after 5 h of starvation. Average numbers of puncta and puncta diameters for the different conditions are presented in **Figure 3B**, **iii and iv**. There were larger numbers (= 30, σ = 12.3) of WIPI2 puncta in cells expressing IBV NSP6-mCherry, and numbers increased (= 38, σ = 20.7) in response to starvation (**Fig. 4B**, **iii**) but the puncta were smaller (= 0.48 μm, σ = 0.11) in diameter compared with those induced by starvation (= 0.66 μm, σ = 0.13, **Fig. 4B**, **iv**). Thus ER-tethered IBV NSP6-mCherry prevents the expansion of WIPI2 puncta in nutrient media and following starvation in HBSS. The results suggest that NSP6 proteins may limit omegasome expansion and modulate autophagosome size before release of autophagosomes into the cytosol.

IBV NSP6 protein does not affect recruitment of SQSTM1 to autophagosomes

The ability of autophagosomes induced by NSP6 to take up cellular cargo was tested by immunostaining for SQSTM1/

Figure 3 (See next page). Effect of IBV NSP6 on maturation of autophagosomes induced by starvation. (**A**) Analysis of fixed cells. Vero cells expressing IBV NSP6-mCherry or infected with IBV were transferred from nutrient media to HBSS and fixed after 4 h. Autophagosomes were visualized by immunofluorescence staining for endogenous MAP1LC3B. Pixel densities in fluorescent images were analyzed in Imaris using spot function to generate rendered images (the images are projections made of 9 z slices 300 nm apart). The diameters of MAP1LC3B-puncta were color coded using the heat map, red puncta represent puncta 1.0 μm or greater. Rendered images are shown below the fluorescence micrographs. Cells expressing NSP6-mCherry, or infected with IBV are outlined with white lines, infected cells were detected by immunostaining for double-stranded RNA (dsRNA), mCherry signals and dsRNA are pseudocolored in black in rendered images. (**B**) Analysis of autophagosome numbers and diameters. The diameters (**i**) and numbers (**ii**) of GFP-MAP1LC3B puncta per cell were calculated from ≥ 20 cells and plotted with the error bars representing the standard deviation. Significant differences in puncta diameter and pucta per cell were measured by a paired *t* test. ***A significant difference of $P < 0.0001$; **a significant difference of $P < 0.001$; *a significant difference of $P < 0.01$. (**C**) Analysis of autophagosome diameter and lifetime. Vero cells were transduced with an adenovirus expressing mammalian GFP-MAP1LC3B. The following day the cells were transferred to HBSS and autophagosome diameters and lifetimes were calculated from time-lapse imaging of GFP-MAP1LC3B puncta. Each data point represents an individual autophagosome. The lifetimes of GFP-MAP1LC3B puncta generated under the indicated conditions are plotted against maximum vesicle diameter. The vertical bar represents 0.75 μm which would provide orange spheres in rendered images. Charts (**i–iv**); control cells transferred to HBSS. Chart(**v and vi**); cells expressing NSP6 transferred to HBSS. Insets indicate numbers of puncta (n), mean diameters (D) and mean lifetimes (L).

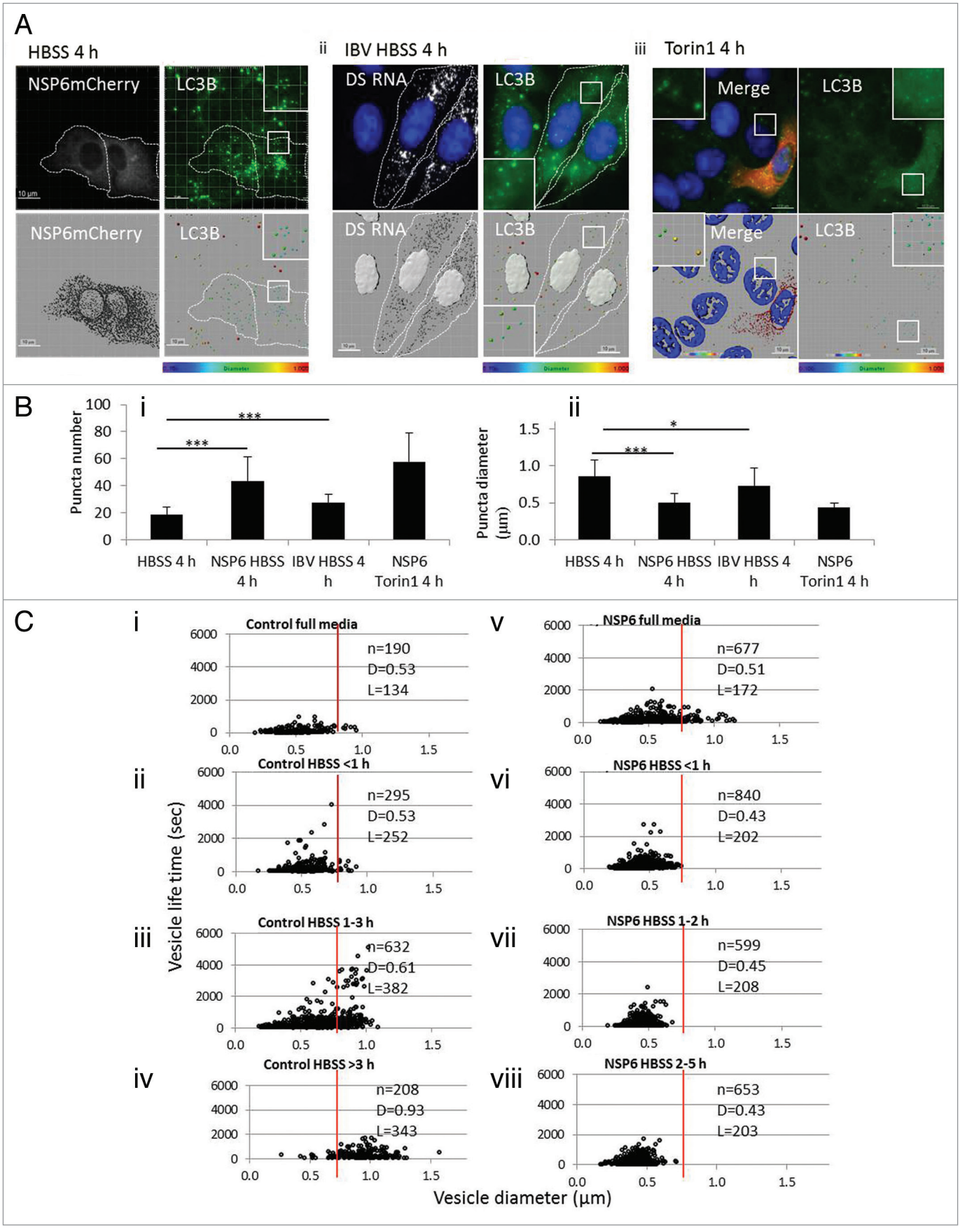

Figure 3. For figure legend, see page 1431.

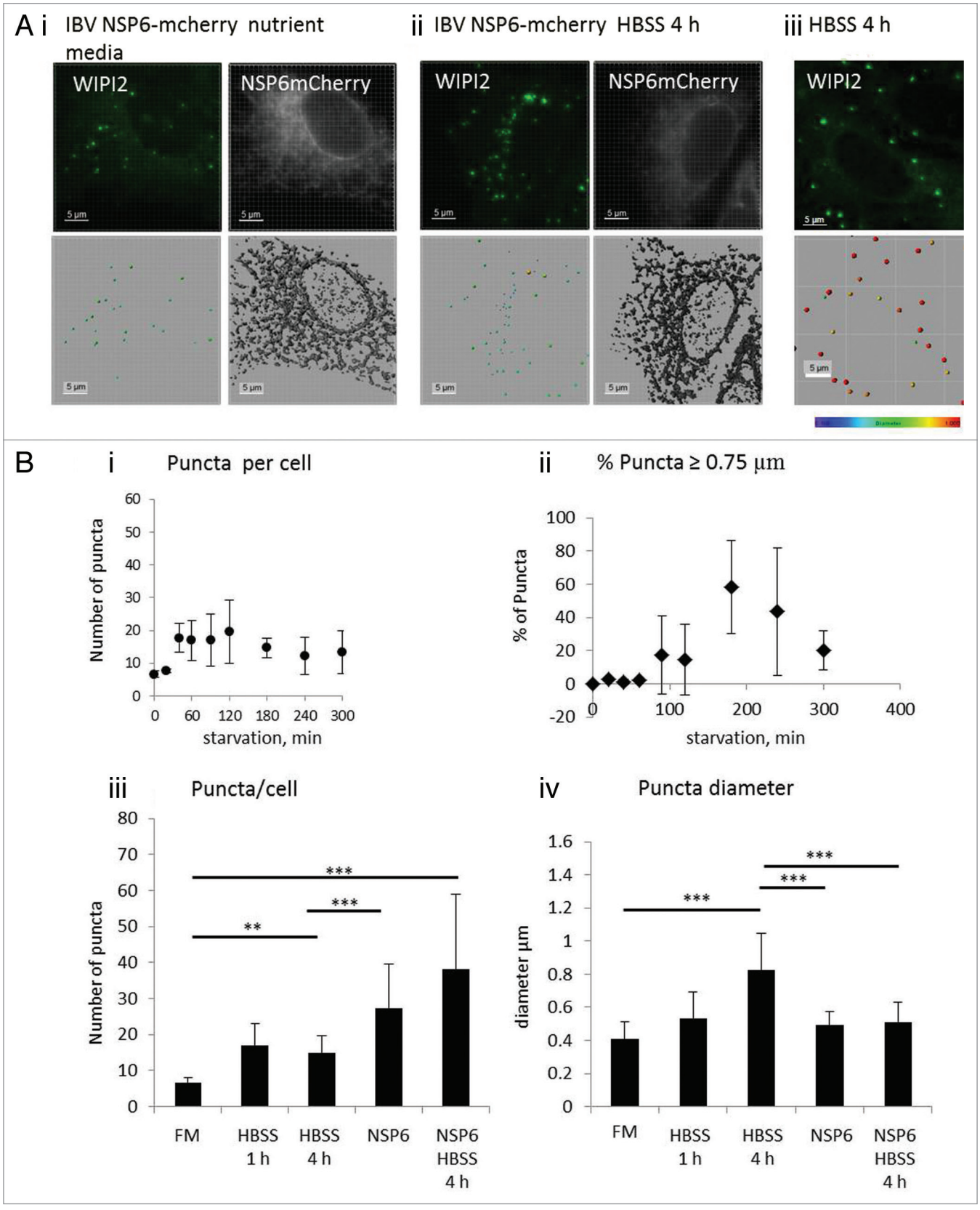

Figure 4. For figure legend, see page 1434.

Figure 4 (See previous page). Effect of IBV NSP6 on maturation of omegasomes. Vero cells were transferred from nutrient media to HBSS and fixed at the indicated times. Omegasomes were visualized by immunofluorescence staining for endogenous WIPI2. Pixel densities in fluorescent images were analyzed in Imaris using spot function to generate rendered images presented below the corresponding fluorescent images (the images are projections made of 9 z slices 300 nm apart). The diameters of WIPI2 puncta were color coded using a heat map red puncta are 1.0 μm or greater. The images show examples from 3 replicate experiments. (**A**) Immunofluorescence images. (**i**) Cells expressing IBV NSP6 maintained in nutrient media, (**ii**) cells expressing IBV NSP6 4 h after transfer to HBSS, (**iii**) control cells 4 h after transfer to HBSS. (**B**) Analysis of omegasome numbers and diameters. The numbers per cell (**i**) and % of WIPI2 puncta with a diameter greater than 0.75 μm (**ii**) were calculated from ≥ 17 cells per time point taken from 3 starvation time courses and plotted with the error bars representing the standard deviation. Composite data were calculated from 3 replicate experiments. Nutrient media (FM): 164 puncta from 21 cells, HBSS 4 h: 127 puncta from 17 cells, IBV NSP6-mCherry in nutrient media: 599 puncta from 26 cells, IBV NSP6-mCherry after 4 h HBSS: 641 puncta from 17 cells. Significant differences in puncta numbers (**iii**) and diameters (**iv**) were measured by a paired *t* test. ***Significant difference of $P < 0.0001$; **a significant difference of $P < 0.001$; *a significant difference of $P < 0.01$.

p62 (SQSTM1), a linker protein that binds ubiquitin and MAP1LC3. The distributions of SQSTM1 and MAP1LC3B were compared in cells incubated in nutrient media, or following transfer to HBSS in the presence or absence of IBV NSP6 (**Fig. 5**). SQSTM1 puncta (red) and MAP1LC3B puncta (green) were rendered and analyzed for degree of colocalization (yellow). Many SQSTM1 puncta were observed in cells in nutrient media (**Fig. 5A**) and most (73%) were red and therefore lacked MAP1LC3B signal. The majority (62%) of SQSTM1 puncta, however, became positive for MAP1LC3B following transfer of cells to HBSS for 1 and 4 h (**Fig. 5C and E**) indicating transfer of SQSTM1 to autophagosomes. Endogenous SQSTM1 puncta were also observed in cells in nutrient media expressing IBV NSP6 (**Fig. 5B**), and the majority (62%) were positive for MAP1LC3B. Double-positive puncta were also formed when cells expressing NSP6 were transferred to HBSS for 1 and 4 h (**Fig. 5D and F**). When SQSTM1 and MAP1LC3B puncta were analyzed from 3 replicate experiments (**Fig. 5G**), there was no observable difference in the recruitment of MAP1LC3B to SQSTM1 puncta in cells expressing NSP6 compared with cells starved by transfer to HBSS. The ability of autophagosomes to degrade SQSTM1 was tested by western blot (**Fig. 5H**). SQSTM1 levels fell by half when cells were starved in HBSS for 4 h, and were reduced to the same extent when cells expressing NSP6 were starved in HBSS or incubated with Torin1. The results showed that small diameter autophagosomes induced by NSP6 can take up SQSTM1 and deliver the protein to lysosomes.

IBV NSP6 protein prevents autolysosome expansion in response to starvation

Autophagosomes formed in response to starvation fuse with multiple lysosomes resulting in consumption of lysosomes into a relatively small number of large autolysosomes.[30] The response of lysosomes to starvation is shown in **Figure 6A**, which compares LAMP2 staining in cells maintained in nutrient media (**Fig. 6A**, **i**) with cells starved for 4 h in HBSS (**Fig. 6A**, **iii**). Fluorescent images gained from LAMP2 immunostaining did not generate puncta that could be rendered to generate spherical images, instead LAMP2 staining was treated as a "surface" (which does not restrict the rendering shape to spheres) to obtain representative images. Regions of interest taken from fluorescence images (**Fig. 6A**, **i and iii**) and corresponding rendered surfaces (**Fig. 6A**, **ii and iv**) show that, consistent with the observations of Yu et al.,[30] lysosomes fall in number and increase in size following starvation in HBSS. The experiment was repeated for cells expressing NSP6-mCherry (**Fig. 6B**). A side-by-side comparison of cells positive (red outline) or negative (white outline) for IBV NSP6-mCherry showed that LAMP2 staining was located to large numbers of small structures when cells were maintained in nutrient media (**Fig. 6B**, **i and ii**), however structures containing LAMP2 failed to grow in size following starvation when cells expressed IBV NSP6-mCherry (**Fig. 6B**, **iii and iv**).

IBV NSP6 protein reduces association of MTOR with lysosomes

The MTOR kinase is regulated by an amino acid-dependent cycle of binding to the Ragulator-RAG complex tethered to the cytoplasmic face of lysosomes. In nutrient media amino acids promote the binding of MTORC1 to the Ragulator-RAG complex leading to activation of MTOR and inhibition of autophagy. When amino acids are removed, MTORC1 dissociates from the Ragulator-RAG complex to the cytosol where it is inactive. The consequent activation of autophagy completes the cycle by generating amino acids from protein degradation in autolysosomes allowing MTOR to return to the Ragulator-RAG complex. This cycle of MTOR association with lysosomes is shown in **Figure 7** where lysosomes were identified by expression of GFP-LAMP1. In nutrient media controls (**Fig. 7A**, **i**) several lysosomes were positive for MTOR (red). The lysosomes lacked MTOR after 1 h incubation in HBSS (**Fig. 7B**, **i**), but MTOR returned to lysosomes at 4 h (**Fig. 7C**, **i**). When the experiment was repeated for cells expressing NSP6, MTOR was missing from the surface of lysosomes in cells in nutrient media (**Fig. 7A**, **ii**) or following 1 (**Fig. 7B**, **ii**) and 4 h (**Fig. 7C**, **ii**) incubations with HBSS. The results suggest that NSP6 may inhibit amino-acid dependent recruitment of MTOR to the surface of lysosomes.

Discussion

This study has examined the properties of autophagosomes induced by coronavirus NSP6 proteins. Autophagosomes were identified by immunostaining for endogenous MAP1LC3B, or by analysis of GFP-MAP1LC3B puncta. Pixel densities obtained from fluorescence images were rendered allowing a statistical comparison with autophagosomes formed in response to starvation. Cells expressing NSP6 proteins contained significantly larger number of autophagosomes (= 54, σ = 15.07) when compared with cells starved in HBSS, however, the autophagosomes induced by NSP6 were significantly smaller in diameter (= 0.48 μm, σ = 0.11) compared with starvation controls (= 0.85 μm, σ = 0.22). At first this suggested that NSP6 proteins had an

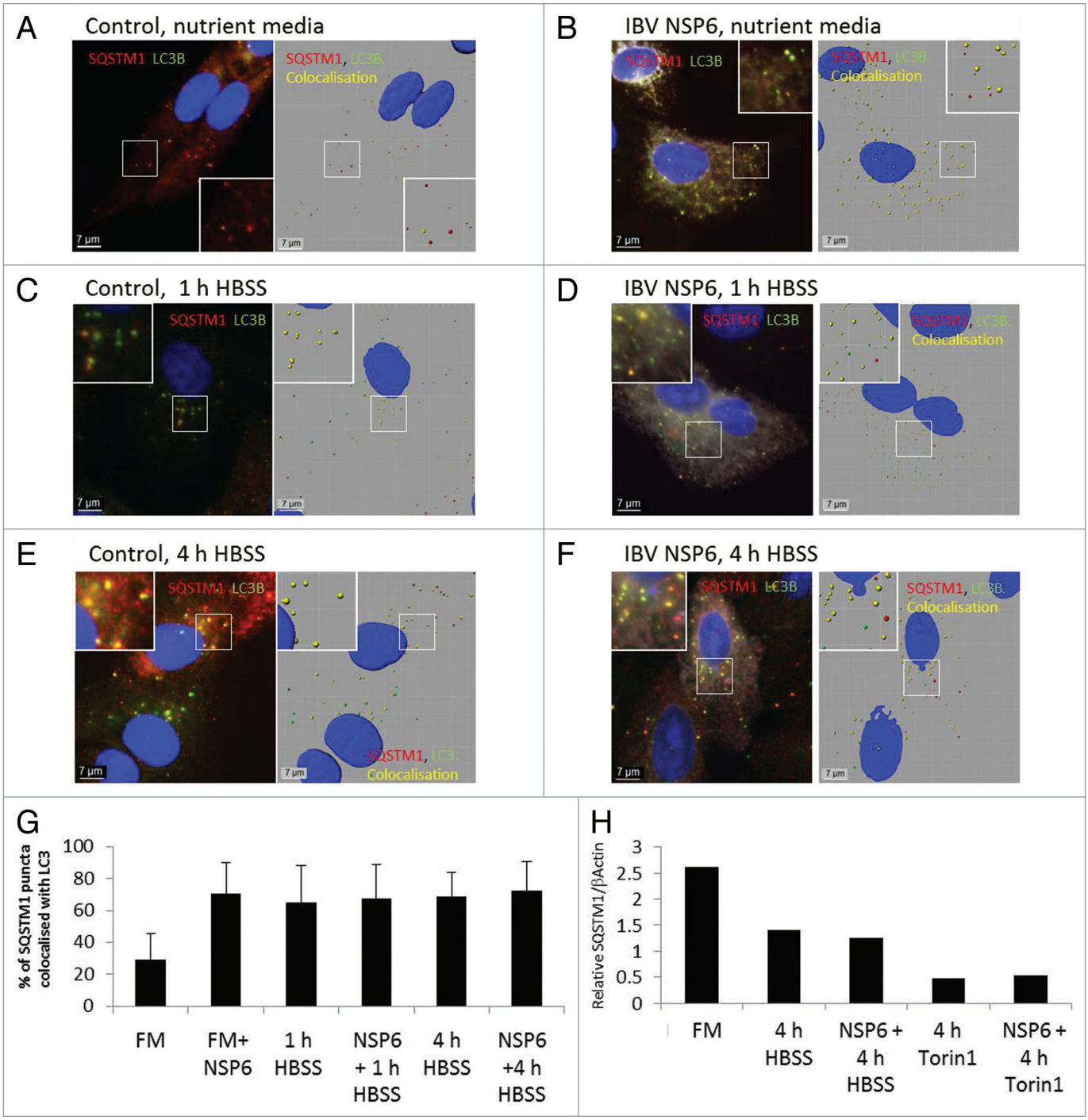

Figure 5. Effect of IBV NSP6 on incorporation of SQSTM1 into autophagosomes. (**A–F**) Vero cells, or Vero cells expressing IBV NSP6, were transferred from nutrient media to HBSS and fixed at the indicated times. Autophagosomes were visualized by immunofluorescence staining for endogenous MAP1LC3B (green) and endogenous SQSTM1 (red). Regions of interest are indicated by white boxes. SQSTM1 puncta (red) and MAP1LC3B puncta (green) were rendered and analyzed for degree of colocalization (yellow). (**G**) SQSTM1 and MAP1LC3B puncta were analyzed from 3 replicate experiments and extent of colocalization of SQSTM1 with MAP1LC3B determined from rendered images. (**H**) Vero cells, or Vero cells expressing IBV NSP6, were transferred from nutrient media to HBSS, or incubated with Torin1 as indicated. Cells were lysed and analyzed for SQSTM1 by western blot. Bar graphs show SQSTM1 levels relative to β-actin.

inherent ability to limit the size of autophagosomes. However, cells expressing NSP6 were maintained in nutrient media, making it possible that nutrient media (rather than NSP6 itself) may limit autophagosome size. A time-course study showed that LC3 puncta formed in nutrient media, or at early times following transfer to HBSS, had small diameters and that autophagosomes with diameters greater than 0.75 μm were only seen in large numbers between 2 and 3 h following transfer to HBSS. This made

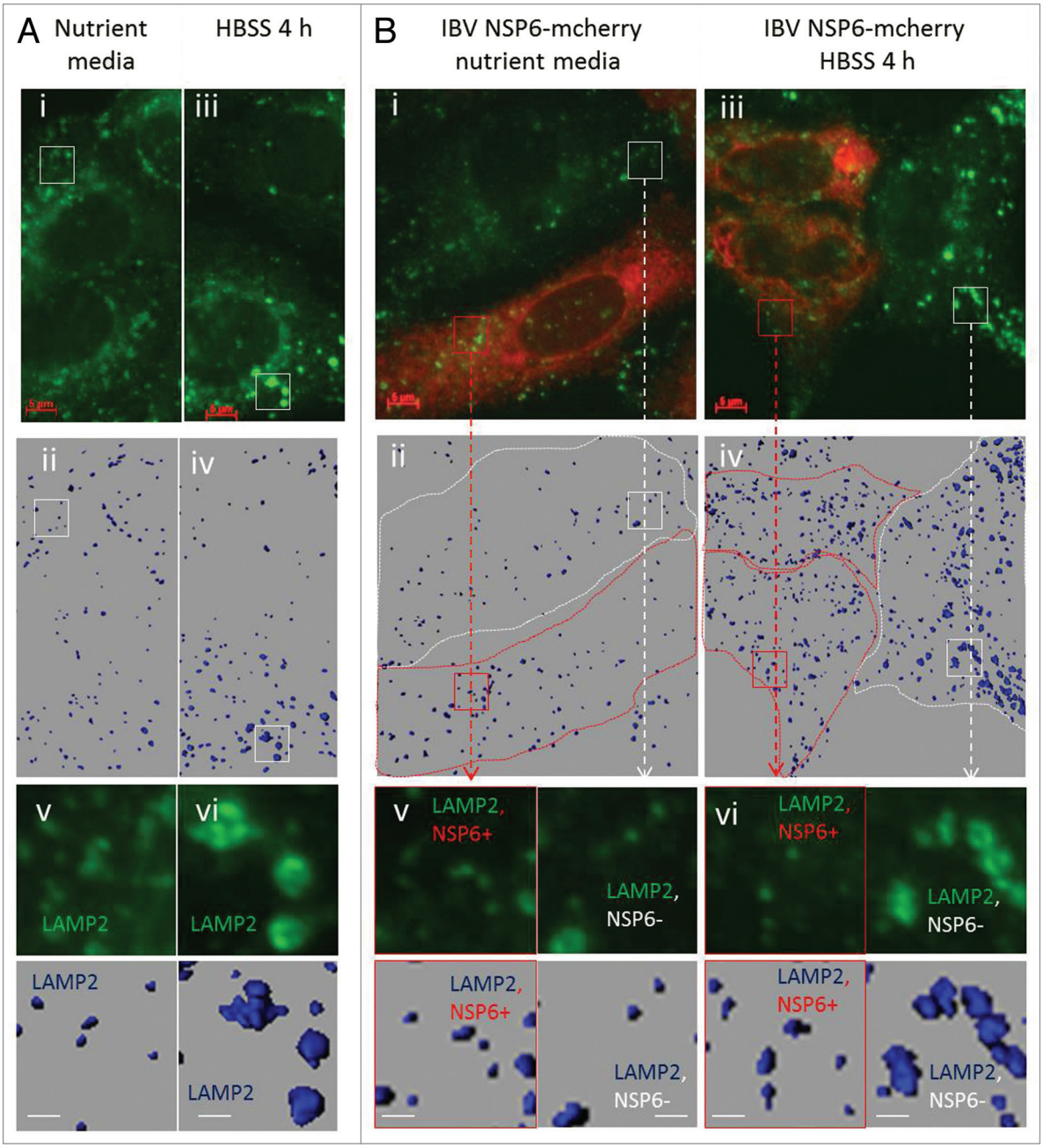

Figure 6. Effect of IBV NSP6 on lysosome and autolysosome expansion in response to starvation. Vero cells, or Vero cells expressing NSP6, were transferred from nutrient media to HBSS and fixed at the indicated times. Lysosomes were visualized by immunofluorescence staining for endogenous LAMP2 (green). IBV NSP6 expression was detected from mCherry tag (red). (**A**) Vero cells. Immunofluorescence images show cells maintained in nutrient media (**i**) or following 4 h in HBSS (**iii**). Rendered images (**ii and iv**) show LAMP2 staining pseudocolored blue using the surfaces function in Imaris. Regions of interest are indicated by white boxes with corresponding high magnification images presented at the bottom of each panel. High magnification images show side-by-side comparisons of regions of interest taken from cells in nutrient media (**v**), or following 4 h in HBSS (**vi**). (**B**) Vero cells expressing IBV NSP6-mCherry. Immunofluorescence images show cells maintained in nutrient media (**i**) or following 4 h in HBSS (**iii**). Rendered images (**ii and iv**) show LAMP2 staining pseudocolored blue using the surfaces function in Imaris. Cells expressing NSP6 are outlined in red, and the region of interest is identified by the red box. Cells negative for NSP6 are outlined in white and region of interest is identified by the white box. High magnification images show side-by-side comparisons of the region of interest taken from cells in nutrient media (**v**), or following 4 h in HBSS (**vi**).

it possible that it took 2 h for autophagosomes to reach 0.75 to 1.0 μm in diameter, or that autophagosome expansion was limited at earlier times. A careful study showed that autophagosomes had similar life times, averaging 8 to 10 min, regardless of whether they were generated in nutrient media, or following 3 h starvation. It did not therefore take 2 h for individual autophagosomes to reach 0.75 to 1.0 μm diameter, and it was possible to conclude that autophagosome expansion was a property of autophagosomes generated after prolonged (2 h) starvation. The effect of IBV NSP6 on the diameters of autophagosomes induced

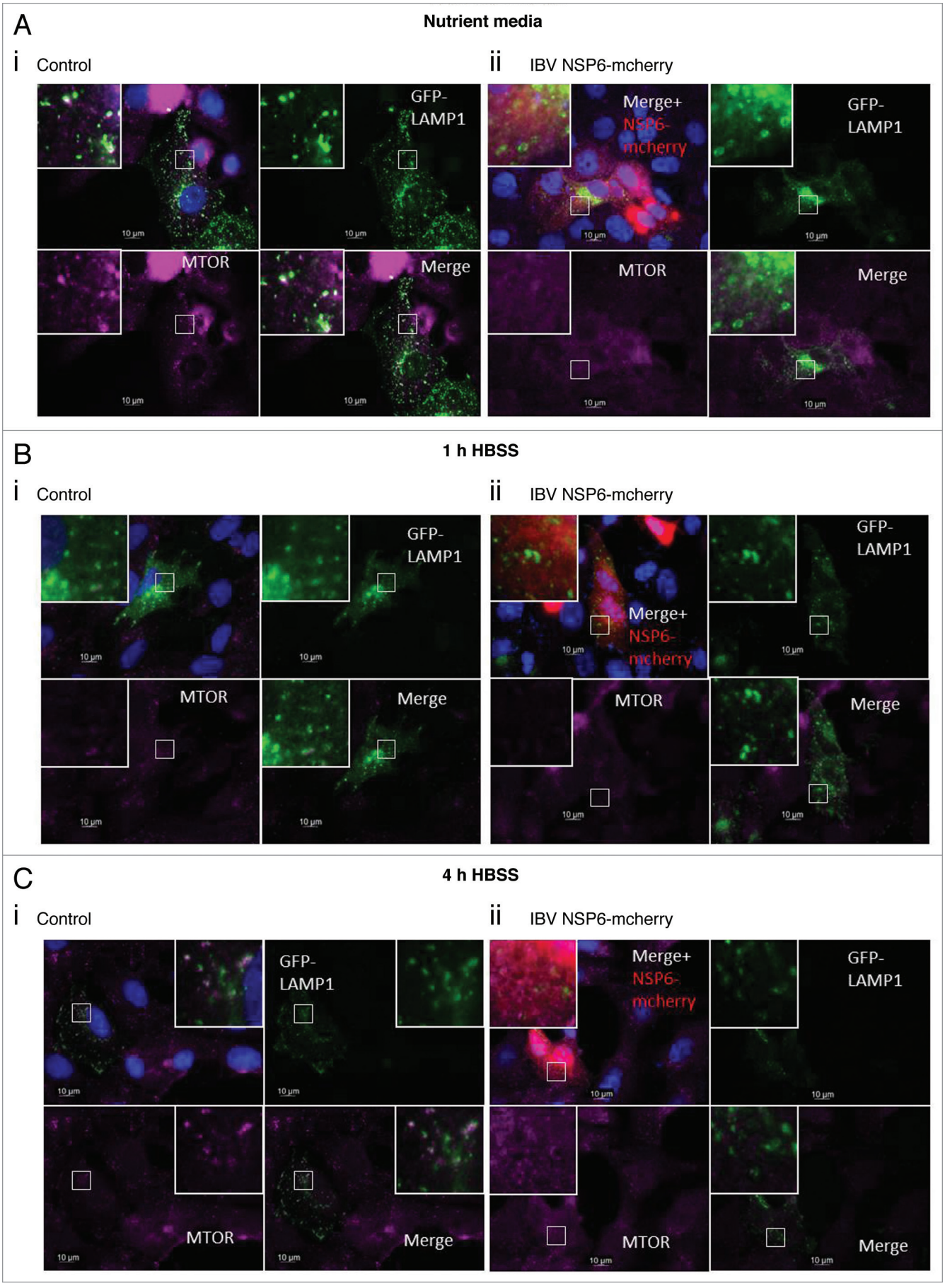
A
Nutrient media
i Control
ii IBV NSP6-mcherry
GFP-LAMP1
Merge+ NSP6-mcherry
MTOR
Merge
10 μm
B
1 h HBSS
i Control
ii IBV NSP6-mcherry
GFP-LAMP1
Merge+ NSP6-mcherry
MTOR
Merge
10 μm
C
4 h HBSS
i Control
ii IBV NSP6-mcherry
GFP-LAMP1
Merge+ NSP6-mcherry
MTOR
Merge
10 μm

Figure 7 (See previous page). Effect of IBV NSP6 on MTOR association with lysosomes in response to starvation. Vero cells, or Vero cells expressing NSP6, were transferred from nutrient media to HBSS and fixed at 1 and 4 h. Lysosomes were visualized by expression of GFP-LAMP1 (green). IBV NSP6 expression was detected from mCherry tag (red). MTOR was detected by immunostaining (far-red). Regions of interest are indicated by white boxes with corresponding high magnification merged images presented at the top left of each panel. (**A**) Nutrient media; (**B**) 1 h in HBSS; (**C**) 4 h in HBSS.

at 2 and 4 h of starvation, or in cells incubated with Torin1, was therefore tested and in each case NSP6 was able to limit the diameter of autophagosomes to the = 0.49 μm, σ = 0.11 seen in cells in nutrient media. Taken together the results show that IBV NSP6 had an inherent ability to limit autophagosome expansion. This restriction is imposed when autophagosomes are induced by NSP6 itself in nutrient media, or when autophagosomes are induced by starvation or chemical inhibition of MTOR signaling, and this property was shared by NSP6 proteins of MHV, SARS, and NSP5-7 of arterivirus PRRSV.

Our previous study has shown that IBV and MHV NSP6 proteins locate to the ER and generate autophagosome via an omegasome intermediate.[28] This pathway of autophagosome induction is dependent on ATG5 and the class III PtdIns3 kinase PIK3C3 and is characterized by the recruitment of double-FYVE-containing protein (ZFYVE1-GFP) to ER domains enriched for PtdIns3P. These domains induced by NSP6 recruit PtdIns3P effector proteins such as WIPI2 to facilitate recruitment of LC3-II to autophagosomes. Interestingly, IBV and MHV NSP6 proteins locate to the ER, but do not colocalize with LC3-II, and do not therefore travel with autophagosomes into the cytosol.[28] Their ability to prevent autophagosome maturation is not therefore dependent on incorporation into the autophagosome membrane, raising the possibility that NSP6 may influence early events in autophagosome formation that occur while the phagophore is still tethered to the ER. WIPI2 binds PtdIns3P and colocalizes with ZFYVE1-GFP during autophagosome formation and is a marker for omegasomes.[6] This allowed us to characterize WIPI2 puncta to follow the effects of NSP6 on omegasome expansion. Following transfer to HBSS for 3 h WIPI2 puncta increased in diameter from 0.2 μm up to 1 μm, with 58% of puncta having a diameter ≥ 0.75 μm. WIPI2 puncta induced by NSP6 were greater in number compared with the starvation control, but as seen for MAP1LC3B puncta, they did not reach the 0.75 to 1 μm diameter produced with starvation. Importantly, WIPI2 puncta formed in cells expressing NSP6 in response to starvation were also of small diameter. The results suggest that NSP6 limits autophagosome diameter at the point of omegasome expansion whether induced directly by NSP6, or independently following inhibition of MTOR signaling induced by starvation.

SQSTM1 is an 'autophagy receptor' protein that has a MAP1LC3-interacting domain that binds MAP1LC3B and an ubiquitin-binding domain to facilitate delivery of ubiquitinated proteins, organelles, and ubiquitin-tagged microbes to autophagosomes.[31] The MAP1LC3B puncta induced following NSP6 expression incorporated SQSTM1, showing that their limited diameter did not affect the recruitment of autophagy cargo binding proteins. Furthermore, SQSTM1 levels fell by half when cells were starved in HBSS for 4 h, and were reduced to the same extent when cells expressing NSP6 were starved in HBSS or incubated with Torin1. The small diameter autophagosomes induced by NSP6 can therefore incorporate SQSTM1 and, and by implication autophagy cargoes, and deliver autophagy cargo to lysosomes. While it seems likely that autophagosomes of 0.5 μm diameter would be able to take up aggregated proteins or viruses (0.06 to 0.2 μm), it remains to be determined if the autophagosomes can accommodate relatively large structures such as mitochondria or bacteria (1to 2.0 μm).

Our results also show that LAMP2 positive structures failed to grow in size following starvation when cells expressed IBV NSP6. LAMP2 is a marker for lysosomes and is incorporated into autolysosomes following fusion with autophagosomes. The lysosome-autolysosome expansion seen in response to autophagy is thought to result from fusion of lysosomes with multiple autophagosomes.[30] The failure of lysosome expansion seen in cells expressing NSP6 could arise if the small autophagosomes failed to fuse with lysosomes. This is unlikely because our previous work shows that MAP1LC3B puncta induced by NSP6 fuse with lysosomes.[28] Autolysosome-lysosome expansion in the presence of NSP6 may therefore be limited because small diameter autophagosomes are unable to fuse with multiple lysosomes.

The activity of MTOR kinase is regulated by the Ragulator-RRAG complex tethered to the cytoplasmic face of lysosomes. Amino acids promote the binding of MTORC1 to the Ragulator-RAG complex leading to activation of MTOR and inhibition of autophagy. When amino acids are removed during starvation MTORC1 dissociates from the Ragulator-RAG complex in an inactive form and this activates autophagy. MTOR returns to the Ragulator-RAG complex when amino acids are generated following fusion of autophagosomes with lysosomes. It was possible to follow this cycle of MTOR association with lysosomes in response to starvation in control cells. We were, however, unable to detect association of MTOR with lysosomes in cells expressing NSP6 and conclude that NSP6 in some way inhibits translocation of MTOR to lysosomes in response to amino acids. It was possible that displacement of MTOR from the Ragulator-RRAG complex by NSP6 might lead to inactivation of MTOR, but this is unlikely because our previous study shows that MTOR signaling, as assessed by phosphorylation MTOR substrate EIF4EBP1/4E-BP1, is not affected by NSP6. Further work is required to determine how cells maintain MTOR signaling without access to the Ragulator-RAG complex on the lysosome. One possibility is that NSP6 alters the distribution of the Ragulator-RAG complex allowing activation of MTOR elsewhere.

The effect of infectious bronchitis virus infection on autophagosome and omegasome diameter was also studied. MAP1LC3B and WIPI2 puncta in cells infected with IBV were significantly smaller than those found in control-starved cells. However, the effect was not as extreme as that seen upon NSP6 expression, perhaps due to the lower amounts of the protein present. This demonstrates that the virus itself has the ability to manipulate omegasome and autophagosome expansion in a

manner that parallels the action of the NSP6 when expressed alone. The actual induction of autophagy in infected cells could, however, be due to other factors of virus infection, such as the presence of double-stranded RNA within the cell, activation of Toll receptor signaling during cell entry and/or induction of ER stress during replication and envelopment. It is also possible that some of the MAP1LC3B puncta seen during infection may be formed by an EDEMosome pathway that is independent of autophagy, and involves direct recruitment of nonlipidated LC31 from the cytosol to ER-derived membranes containing viral replicase proteins.[32,33]

Autophagy is activated during coronavirus infection[28,34,35] but the precise reasons why coronaviruses would limit subsequent autophagosome expansion is unclear. Much work has focused on the potential role of autophagosomes in generating sites of coronavirus replication. Early work with cells from *atg5*$^{-/-}$ mice suggested that autophagy may be required for replication of MHV in mouse embryonic cells,[34] but later work showed that replication of MHV in macrophages or primary fibroblasts does not require *Atg5* or *Atg7*.[33,36] Double-membrane vesicles (DMVs) resembling autophagosomes are seen in large numbers in the cytoplasm of cells infected with coronaviruses and arteriviruses.[14,26,27] The DMVs are 250 ± 50 nm in diameter and are much smaller that autophagosomes formed during starvation (850 ± 22 nm), but are closer to the diameter of the autophagosomes induced by NSP6. One possibility is that DMVs result from restricted autophagosome expansion induced by NSP6. It has been proposed that viral RNA may be sequestered within DMVs and protected from recognition by host defenses activated by dsRNA. While small autophagosomes induced by NSP6 may generate DMVs, it is unlikely that they sequester viral RNA genomes because the MAP1LC3B puncta induced during IBV infection do not colocalize with dsRNA.[28] More work will be needed to understand the relationship between DMVs, small diameter autophagosomes, and MAP1LC3 positive EDEMosomes during coronavirus replication. Autophagy can, nevertheless, be triggered during viral infection following recognition of viral nucleic acids by Toll-like receptors and/or activation of cell stress pathways such as ER stress. Autophagy has the potential to capture and degrade viruses and virus components. Although the SQSTM1 flux data do not support a global suppression of degradative capacity, it is possible that certain viral components may escape degradation leading to reduced antigen presentation and/or exposure to Toll-like receptors. Alternatively, NSP6 may activate autophagy from the ER to remove host proteins that would inhibit replication, for example immunomodulatory proteins synthesized in the ER and then secreted by cells in response to infection.

Materials and Methods

Cells, virus, and reagents

VERO cells (ECACC, 84113001), were obtained from the European Collection of Cell Cultures (ECACC). Cells were grown at 37 °C with 5% CO_2. Cells were starved by incubating in Hank's balanced salt solution (HBSS; Invitrogen, 14025-076) for the specified length of time. Infectious bronchitis virus (IBV), the Beaudette Beau-R isolate, was provided by the Institute for Animal Health (IAH), Compton Laboratory. Constructs IBV NSP6-mCherry and MHV NSP6-mCherry have been described previously.[28] The adenovirus mammalian GFP-MAP1LC3B construct has been described previously.[37] Primary antibodies used for immunofluorescence were as follows: rabbit_anti-MAP1LC3B (Sigma L7543), mouse_anti-WIPI2 (Abcam, ab101985), mouse_H4B4_anti-LAMP2 (Abcam ab25631), mouse_J2_anti-dsRNA (English and Scientific Consulting Bt. 10010200), guinea pig anti-SQSTM1/p62 (PROGEN Biotechnik, GP62-C).

Transfections and transductions

Cells were seeded onto glass coverslips, and then transfected/transduced the following day. Cells were transfected using jetPRIME (Polyplus transfection, 114-01), and the transfection mix was washed off after 4 h, and assayed 24 h later. Replication defective Ad5 adenovirus was prepared by infection of competent HEK 293A cells expressing E1. Cells were grown for 2 to 3 d until signs of cytopathic effect. Virus was released by 2 cycles of freeze thaw followed by centrifugation (15 min at 1620 G) to remove cell debris. Cells were transduced with adenovirus over night by addition of recombinant adenovirus stock to complete media. Virus stocks were titrated to determine volume required to transduce 80% to 90% of target cells. It has previously been shown that puncta are not seen in cells transduced with an adenovirus expressing GFP alone in complete media or starvation media.[38]

Imaging and Imaris image analysis

Cells were fixed using 100% ice-cold methanol. Cells were stained using antibodies at a 1:1,000 dilution in 2% bovine serum albumin (Sigma, A9418) in phosphate-buffered saline (OXOID, BR0014G) Nuclei were counterstained with DAPI (Thermo Scientific, 62248). The fixed cell images were obtained at ×63 magnification on a Zeiss Axioplan microscope with a 63×, 1.4 NA oil-immersion objective (Zeiss, Oberkochen, Germany), 2 taking 9 z stacks 300 nm apart, which completely encompassed the breadth of the cells, unless otherwise stated. Live cells were imaged using a Zeiss LSM510 META confocal microscope (Zeiss, Oberkochen, Germany). Z stacks were not taken during the live-cell imaging because they could not be taken at a faster speed than the autophagosomes moved.

Images were analyzed using the IMARIS package (BITPLANE Scientific Software). The spot function was used to identify and measure the diameter of fluorescent puncta using the whole z stack for each experiment. The spot function creates spherical spots which are a computer-generated representation or rendering of the region of interest. The regions are identified by using local contrast, and seed points are calculated to mark each individual spot allowing the spot to be visualized as an artificial solid sphere. The software allows the user to verify the accuracy of the spot segmentation against the original fluorescence intensity data. A spot is a region of a digital image in which some properties are constant or vary within a prescribed range of values; all the points in a spot can be considered in some sense to be similar to each other. An expected spot diameter was defined as 0.4 μm. A Gaussian filter was used to remove background noise, smoothing over objects at a distance below 8/9 of the expected spot radius.

The center of each spot or seed point could then be identified confidently. Local contrast was then used to estimate spot size as this can account for variations in background intensity, whereas absolute intensity of pixels will not. This process uses a Laplacian filter in conjunction with the Gaussian function (LoG) to identify areas of rapid change or edges. The LoG operator makes a derivative of the image where areas of uniform intensity are equal to zero, and when change occurs positive or negative values are introduced. Thus a spot circumference can be detected by the sharpness of change in intensity, not the absolute intensity, and is hence independent of background fluorescence intensity. The rendered images of the LC3 puncta and WIPI2 puncta are colored according to diameter on a graded scale with a diameter of 0.1 μm being blue, and anything 1 μm and above being colored red. The surfaces function (which acts in a similar way to the spots function, only the objects are not limited to being spheres) was used to render the ER staining of the membrane localized IBV NSP6-mCherry, and also the endogenous LAMP2 stain. Tracking of fluorescent puncta/vesicles was performed in Imaris (an example is shown in **Vid. S5**). For lifetime analysis, autoregressive motion was used to track puncta with a distance of 1 μm being used to determine spots traveling between frames. Average diameter and average duration were used for analysis of each puncta. The data was tested for statistical significance using the paired 2-tailed Student *t* test.

Western blot

Cell lysates denatured in SDS were separated on 4–12% Bis-Tris gels (Novex, NP0322BOX). Proteins were transferred on to PVDF membranes and probed using guinea pig anti-SQSTM1/p62 (PROGEN Biotechnik, GP62-C) and Mouse anti-β-Actin (Sigma, AC-15). Mouse 800 (LI-COR 926-32210) and guinea pig 680 (LI-COR 926-3241) were visualized with a LI-COR Odyssey Infrared imager (LI-COR Cambridge, UK).

Disclosure of Potential Conflicts of Interest

No potential conflicts of interest were disclosed.

Acknowledgments

The work reported here was funded by BBSRC grant BB/E018521/1 to TW.

Supplemental Materials

Supplemental materials may be found here:
www.landesbioscience.com/journals/autophagy/article/29309

References

1. Wang CW, Klionsky DJ. The molecular mechanism of autophagy. Mol Med 2003; 9:65-76; PMID:12865942
2. Zhong Y, Wang QJ, Li X, Yan Y, Backer JM, Chait BT, Heintz N, Yue Z. Distinct regulation of autophagic activity by Atg14L and Rubicon associated with Beclin 1-phosphatidylinositol-3-kinase complex. Nat Cell Biol 2009; 11:468-76; PMID:19270693; http://dx.doi.org/10.1038/ncb1854
3. Matsunaga K, Morita E, Saitoh T, Akira S, Ktistakis NT, Izumi T, Noda T, Yoshimori T. Autophagy requires endoplasmic reticulum targeting of the PI3-kinase complex via Atg14L. J Cell Biol 2010; 190:511-21; PMID:20713597; http://dx.doi.org/10.1083/jcb.200911141
4. Hamasaki M, Furuta N, Matsuda A, Nezu A, Yamamoto A, Fujita N, Oomori H, Noda T, Haraguchi T, Hiraoka Y, et al. Autophagosomes form at ER-mitochondria contact sites. Nature 2013; 495:389-93; PMID:23455425; http://dx.doi.org/10.1038/nature11910
5. Axe EL, Walker SA, Manifava M, Chandra P, Roderick HL, Habermann A, Griffiths G, Ktistakis NT. Autophagosome formation from membrane compartments enriched in phosphatidylinositol 3-phosphate and dynamically connected to the endoplasmic reticulum. J Cell Biol 2008; 182:685-701; PMID:18725538; http://dx.doi.org/10.1083/jcb.200803137
6. Proikas-Cezanne T, Waddell S, Gaugel A, Frickey T, Lupas A, Nordheim A. WIPI-1alpha (WIPI49), a member of the novel 7-bladed WIPI protein family, is aberrantly expressed in human cancer and is linked to starvation-induced autophagy. Oncogene 2004; 23:9314-25; PMID:15602573; http://dx.doi.org/10.1038/sj.onc.1208331
7. Polson HE, de Lartigue J, Rigden DJ, Reedijk M, Urbé S, Clague MJ, Tooze SA. Mammalian Atg18 (WIPI2) localizes to omegasome-anchored phagophores and positively regulates LC3 lipidation. Autophagy 2010; 6:506-22; PMID:20505359; http://dx.doi.org/10.4161/auto.6.4.11863
8. Burman C, Ktistakis NT. Regulation of autophagy by phosphatidylinositol 3-phosphate. FEBS Lett 2010; 584:1302-12; PMID:20074568; http://dx.doi.org/10.1016/j.febslet.2010.01.011
9. Suzuki K, Ohsumi Y. Current knowledge of the pre-autophagosomal structure (PAS). FEBS Lett 2010; 584:1280-6; PMID:20138172; http://dx.doi.org/10.1016/j.febslet.2010.02.001
10. Levine B. Eating oneself and uninvited guests: autophagy-related pathways in cellular defense. Cell 2005; 120:159-62; PMID:15680321
11. Cherry S. VSV infection is sensed by Drosophila, attenuates nutrient signaling, and thereby activates antiviral autophagy. Autophagy 2009; 5:1062-3; PMID:19713743; http://dx.doi.org/10.4161/auto.5.7.9730
12. English L, Chemali M, Duron J, Rondeau C, Laplante A, Gingras D, Alexander D, Leib D, Norbury C, Lippé R, et al. Autophagy enhances the presentation of endogenous viral antigens on MHC class I molecules during HSV-1 infection. Nat Immunol 2009; 10:480-7; PMID:19305394; http://dx.doi.org/10.1038/ni.1720
13. Orvedahl A, MacPherson S, Sumpter R Jr., Tallóczy Z, Zou Z, Levine B. Autophagy protects against Sindbis virus infection of the central nervous system. Cell Host Microbe 2010; 7:115-27; PMID:20159618; http://dx.doi.org/10.1016/j.chom.2010.01.007
14. Cottam E, Pierini R, Roberts R, Wileman T. Origins of membrane vesicles generated during replication of positive-strand RNA viruses. Future Virol 2009; 4:473-85; http://dx.doi.org/10.2217/fvl.09.26
15. Jackson WT, Giddings TH Jr., Taylor MP, Mulinyawe S, Rabinovitch M, Kopito RR, Kirkegaard K. Subversion of cellular autophagosomal machinery by RNA viruses. PLoS Biol 2005; 3:e156; PMID:15884975; http://dx.doi.org/10.1371/journal.pbio.0030156
16. Kirkegaard K. Subversion of the cellular autophagy pathway by viruses. Curr Top Microbiol Immunol 2009; 335:323-33; PMID:19802573; http://dx.doi.org/10.1007/978-3-642-00302-8_16
17. Wileman T. Aggresomes and autophagy generate sites for virus replication. Science 2006; 312:875-8; PMID:16690857; http://dx.doi.org/10.1126/science.1126766
18. Orvedahl A, Alexander D, Tallóczy Z, Sun Q, Wei Y, Zhang W, Burns D, Leib DA, Levine B. HSV-1 ICP34.5 confers neurovirulence by targeting the Beclin 1 autophagy protein. Cell Host Microbe 2007; 1:23-35; PMID:18005679; http://dx.doi.org/10.1016/j.chom.2006.12.001
19. Suhy DA, Giddings TH Jr., Kirkegaard K. Remodeling the endoplasmic reticulum by poliovirus infection and by individual viral proteins: an autophagy-like origin for virus-induced vesicles. J Virol 2000; 74:8953-65; PMID:10982339; http://dx.doi.org/10.1128/JVI.74.19.8953-8965.2000
20. Taylor MP, Kirkegaard K. Modification of cellular autophagy protein LC3 by poliovirus. J Virol 2007; 81:12543-53; PMID:17804493; http://dx.doi.org/10.1128/JVI.00755-07
21. Su WC, Chao TC, Huang YL, Weng SC, Jeng KS, Lai MM. Rab5 and class III phosphoinositide 3-kinase Vps34 are involved in hepatitis C virus NS4B-induced autophagy. J Virol 2011; 85:10561-71; PMID:21835792; http://dx.doi.org/10.1128/JVI.00173-11
22. Shelly S, Lukinova N, Bambina S, Berman A, Cherry S. Autophagy is an essential component of Drosophila immunity against vesicular stomatitis virus. Immunity 2009; 30:588-98; PMID:19362021; http://dx.doi.org/10.1016/j.immuni.2009.02.009
23. Chi PI, Huang WR, Lai IH, Cheng CY, Liu HJ. The p17 nonstructural protein of avian reovirus triggers autophagy enhancing virus replication via activation of phosphatase and tensin deleted on chromosome 10 (PTEN) and AMP-activated protein kinase (AMPK), as well as dsRNA-dependent protein kinase (PKR)/eIF2α signaling pathways. J Biol Chem 2013; 288:3571-84; PMID:23233667; http://dx.doi.org/10.1074/jbc.M112.390245
24. Kumar SH, Rangarajan A. Simian virus 40 small T antigen activates AMPK and triggers autophagy to protect cancer cells from nutrient deprivation. J Virol 2009; 83:8565-74; PMID:19515765; http://dx.doi.org/10.1128/JVI.00603-09
25. Cavanagh D. Coronavirus avian infectious bronchitis virus. Vet Res 2007; 38:281-97; PMID:17296157; http://dx.doi.org/10.1051/vetres:2006055

26. Knoops K, Bárcena M, Limpens RW, Koster AJ, Mommaas AM, Snijder EJ. Ultrastructural characterization of arterivirus replication structures: reshaping the endoplasmic reticulum to accommodate viral RNA synthesis. J Virol 2012; 86:2474-87; PMID:22190716; http://dx.doi.org/10.1128/JVI.06677-11
27. Knoops K, Kikkert M, Worm SH, Zevenhoven-Dobbe JC, van der Meer Y, Koster AJ, Mommaas AM, Snijder EJ. SARS-coronavirus replication is supported by a reticulovesicular network of modified endoplasmic reticulum. PLoS Biol 2008; 6:e226; PMID:18798692; http://dx.doi.org/10.1371/journal.pbio.0060226
28. Cottam EM, Maier HJ, Manifava M, Vaux LC, Chandra-Schoenfelder P, Gerner W, Britton P, Ktistakis NT, Wileman T. Coronavirus nsp6 proteins generate autophagosomes from the endoplasmic reticulum via an omegasome intermediate. Autophagy 2011; 7:1335-47; PMID:21799305; http://dx.doi.org/10.4161/auto.7.11.16642
29. Xie Z, Klionsky DJ. Autophagosome formation: core machinery and adaptations. Nat Cell Biol 2007; 9:1102-9; PMID:17909521; http://dx.doi.org/10.1038/ncb1007-1102
30. Yu L, McPhee CK, Zheng L, Mardones GA, Rong Y, Peng J, Mi N, Zhao Y, Liu Z, Wan F, et al. Termination of autophagy and reformation of lysosomes regulated by mTOR. Nature 2010; 465:942-6; PMID:20526321; http://dx.doi.org/10.1038/nature09076
31. Pankiv S, Clausen TH, Lamark T, Brech A, Bruun JA, Outzen H, Øvervatn A, Bjørkøy G, Johansen T. p62/SQSTM1 binds directly to Atg8/LC3 to facilitate degradation of ubiquitinated protein aggregates by autophagy. J Biol Chem 2007; 282:24131-45; PMID:17580304; http://dx.doi.org/10.1074/jbc.M702824200
32. Monastyrska I, Ulasli M, Rottier PJ, Guan JL, Reggiori F, de Haan CA. An autophagy-independent role for LC3 in equine arteritis virus replication. Autophagy 2013; 9:164-74; PMID:23182945; http://dx.doi.org/10.4161/auto.22743
33. Reggiori F, Monastyrska I, Verheije MH, Calì T, Ulasli M, Bianchi S, Bernasconi R, de Haan CA, Molinari M. Coronaviruses Hijack the LC3-I-positive EDEMosomes, ER-derived vesicles exporting short-lived ERAD regulators, for replication. Cell Host Microbe 2010; 7:500-8; PMID:20542253; http://dx.doi.org/10.1016/j.chom.2010.05.013
34. Prentice E, Jerome WG, Yoshimori T, Mizushima N, Denison MR. Coronavirus replication complex formation utilizes components of cellular autophagy. J Biol Chem 2004; 279:10136-41; PMID:14699140; http://dx.doi.org/10.1074/jbc.M306124200
35. Sun MX, Huang L, Wang R, Yu YL, Li C, Li PP, Hu XC, Hao HP, Ishag HA, Mao X. Porcine reproductive and respiratory syndrome virus induces autophagy to promote virus replication. Autophagy 2012; 8:1434-47; PMID:22739997; http://dx.doi.org/10.4161/auto.21159
36. Zhao Z, Thackray LB, Miller BC, Lynn TM, Becker MM, Ward E, Mizushima NN, Denison MR, Virgin HW 4th. Coronavirus replication does not require the autophagy gene ATG5. Autophagy 2007; 3:581-5; PMID:17700057
37. Köchl R, Hu XW, Chan EY, Tooze SA. Microtubules facilitate autophagosome formation and fusion of autophagosomes with endosomes. Traffic 2006; 7:129-45; PMID:16420522; http://dx.doi.org/10.1111/j.1600-0854.2005.00368.x
38. Maier HJ, Cottam EM, Stevenson-Leggett P, Wilkinson JA, Harte CJ, Wileman T, Britton P. Visualizing the autophagy pathway in avian cells and its application to studying infectious bronchitis virus. Autophagy 2013; 9:496-509; PMID:23328491; http://dx.doi.org/10.4161/auto.23465